

Square Gravity

C.F. Baillie

Dept. of Computer Science
University of Colorado
Boulder, CO 80309, USA

and

D.A. Johnston

Dept. of Mathematics
Heriot-Watt University
Riccarton
Edinburgh, EH14 4AS
Scotland

18 June 1995

Abstract

We simulate the Ising model on dynamical quadrangulations using a generalization of the flip move for triangulations with two aims: firstly, as a confirmation of universality for the KPZ/DDK exponents of the Ising phase transition, worthwhile in view of some recent surprises with other sorts of dynamical lattices; secondly, to investigate the transition of the Ising *anti*-ferromagnet on a dynamical loosely packed (bipartite) lattice. In the latter case we show that it is still possible to define a staggered magnetization and observe the anti-ferromagnetic analogue of the transition.

Submitted to Physics Letters B.

1 Theoretical Background

The behaviour of various spin models on dynamical triangulations and their dual planar ϕ^3 graphs has been extensively investigated both analytically [1, 2] and numerically [3, 4] recently because of their interest for string theory and $2d$ gravity. The sum over triangulations or graphs in such models serves as a discretization of the sum over metrics in the continuum theories. In simulations the space of triangulations or their duals is generally sampled by performing local “flip” moves [5], though more recently cluster-like moves for the geometry (“baby-universe surgery”) have been proposed [6]. Considering multiple copies of spin models, or alternatively large Q Potts models, has led to considerable progress in understanding the $c > 1$ regime in $2d$ quantum gravity [7, 8].

The microcanonical partition function for an Ising model on some ensemble of graphs with n vertices is given by

$$Z_n(\beta, H) = \sum_{G^n} \sum_{\{\sigma\}} \exp \beta \left(\sum_{\langle ij \rangle} G_{ij}^n \sigma_i \sigma_j + H \sum_i \sigma_i \right) \quad (1)$$

where G_{ij}^n is the connectivity matrix for the graph G^n . For the particular case of the Ising model on planar ϕ^3 and ϕ^4 graphs the solution proceeds by noting the equivalence of the grand canonical partition function arising from equ.(1) and the free energy of an $N \times N$ two matrix model [1]. In the ϕ^4 case in zero external field this is

$$F_{\phi^4}(c, g, H) = \frac{1}{N^2} \log \left(\int d^{N^2} M_1 d^{N^2} M_2 \exp -tr \frac{N}{g} \left(\frac{M_1^2}{2} + \frac{M_2^2}{2} - c M_1 M_2 + \frac{1}{4} M_1^4 + \frac{1}{4} M_2^4 \right) \right) \quad (2)$$

and for ϕ^3 graphs

$$F_{\phi^3}(c, g, H) = \frac{1}{N^2} \log \left(\int d^{N^2} M_1 d^{N^2} M_2 \exp -tr \frac{N}{g} \left(\frac{M_1^2}{2} + \frac{M_2^2}{2} - c M_1 M_2 + \frac{1}{3} M_1^3 + \frac{1}{3} M_2^3 \right) \right) \quad (3)$$

where $c = \exp(-2\beta)$ introduces the temperature of the spins into the theory. In the planar limit $N \rightarrow \infty$ it is possible to solve the model exactly using orthogonal polynomial or saddle point methods and derive the full set of critical exponents, which are in agreement with those calculated from continuum conformal field theory [2].

It is expected that the Ising model on any dynamical polygonization or its dual will display the KPZ/DDK critical behaviour so long as further couplings are not tuned to give a multicritical point. This has been demonstrated both analytically and numerically for various variants of ϕ^3 graphs where self-energy diagrams and tadpoles are either excluded or not. Although the critical temperature changes, the critical exponents are unaffected. There have, however, been some recent surprises with other discretizations: with $2d$ Regge calculus the Onsager exponents were observed [9]; and with apparently “flat” models the KPZ/DDK exponents were measured [10]. This increases the incentive for performing an explicit check on the behaviour of various possible discretizations.

It is possible to write down explicitly a matrix model for the Ising model on a dynamical triangulation (ie with the spins residing at the vertices of the triangle, rather than in the centre as is effectively the case for ϕ^3 graphs). The action of this model is given by [11]

$$U_{DTRS} = \frac{N}{g} tr \left(\frac{1}{2 \cosh(\beta)(1+c^*)} S^2 + \frac{1}{2 \cosh(\beta)(1-c^*)} D^2 + S^3/3 + SD^2 \right) \quad (4)$$

where $c^* = (1-c)/(1+c)$ is the transformation induced in c by the standard duality transformation on β and S and D are still $N \times N$ hermitian matrices representing edges with the same and different spins at the end respectively. This model may be transformed into a form equivalent to the “ $O(1)$ ” representation of the Ising model on ϕ^3 graphs which is discussed in [12]

$$U_{\phi^3} = \frac{N}{g} tr \left(D^2 S + \frac{S^3}{12} - \frac{c^*}{2} S^2 + \frac{(3c^* - 1)(1 + c^*)}{4} S \right) \quad (5)$$

and shown to have Ising critical behaviour at the dual of the ϕ^3 model transition temperature. Working directly on the triangulations with U_{DTRS} thus provides an explicit confirmation of duality and a further check on the universality of the exponents.

We can carry out a strong coupling expansion whatever the lattice our Ising model inhabits

$$Z_V(\beta, 0) = \sum_{G^V} 2^V (\cosh(\beta))^E \sum_{\text{loops}} (\tanh(\beta))^{\text{length}} \quad (6)$$

where the loop sum is restricted to edges that are only traversed once. This makes it clear that we should only expect to see an *anti*-ferromagnetic transition in the Ising model on lattices where only even loops are possible, because only here do we have a $\beta \rightarrow -\beta$ symmetry. Thus, for instance, the honeycomb lattice in $2d$ displays an antiferromagnetic transition whereas the triangular lattice does not. It is not entirely trivial to conclude that such transitions would survive a coupling to $2d$ gravity, which in effect introduces annealed connectivity disorder into the lattices. Both the analogue of the honeycomb lattice – dynamical ϕ^3 graphs, and the triangular lattice – dynamical triangulations, fail to display an antiferromagnetic transition because both odd and even loops are present.

Graphs with only even loops can be constructed in general by considering complex matrices [13], but we take a slightly different tack here and consider the Ising model on a dynamical quadrangulation, where the action is given by

$$U_{DQRS} = \frac{N}{g} \text{tr} \left(\frac{1}{2} S^2 + \frac{1}{2} D^2 + \frac{g_1}{4} S^4 + \frac{g_2}{4} D^4 + \frac{g_3}{2} (SDSD + 2S^2 D^2) \right) \quad (7)$$

with

$$\begin{aligned} g_1 &= \cosh^2(\beta)(1+c^*)^2 \\ g_2 &= \cosh^2(\beta)(1-c^*)^2 \\ g_3 &= \cosh^2(\beta)(1+c^*)(1-c^*). \end{aligned} \quad (8)$$

This model can be shown to have a transition at $c = 3/5$ by transforming the action back to a form resembling that for the Ising model on ϕ^4 graphs. With some scalings we can rewrite equ.(8) as

$$U_{DQRS} = \frac{N}{g} \text{tr} \left(\frac{1}{2} S^2 + \frac{1}{2} D^2 + \frac{1}{4(1-c^*)^2} S^4 + \frac{1}{4(1+c^*)^2} D^4 + \frac{1}{2(1-c^*)(1+c^*)} (SDSD + 2S^2 D^2) \right). \quad (9)$$

The ϕ^4 model of equ.(2) is recast by setting $A = (M_1 + M_2)/\sqrt{2}$, $B = (M_1 - M_2)/\sqrt{2}$ and then rescaling $A \rightarrow \sqrt{2}A/\sqrt{1-c}$, $B \rightarrow \sqrt{2}B/\sqrt{1+c}$, $g \rightarrow 2g$. This gives

$$U_{\phi^4} = \frac{N}{g} \text{tr} \left(\frac{1}{2} A^2 + \frac{1}{2} B^2 + \frac{1}{4(1-c)^2} A^4 + \frac{1}{4(1+c)^2} B^4 + \frac{1}{2(1-c)(1+c)} (ABAB + 2A^2 B^2) \right). \quad (10)$$

which is identical in form to equ.(9). Given that U_{ϕ^4} produces an Ising transition at $c = 1/4$, comparison with equ.(9) shows that U_{DQRS} produces an Ising transition at $c^* = 1/4$ (ie $c = 3/5$), the quoted result. Furthermore, the possibility of an antiferromagnetic transition is manifested in equ.(9) too as $\beta \rightarrow -\beta$ (ie $c^* \rightarrow -c^*$) is obviously a symmetry of the action upon exchange of S and D . This is *not* the case for the original ϕ^4 action, even in its modified form in equ.(10), as $c \rightarrow 1/c$ when $\beta \rightarrow -\beta$.

The matrix model considerations would thus suggest that the Ising model on dynamical quadrangulations displays an antiferromagnetic transition with the same critical exponents as the ferromagnetic case. This is not a totally vacuous observation, as the antiferromagnetic transition essentially operates on two decoupled sets of Ising spins, so it is not entirely obvious that one should see the exponents for a one Ising model transition coupled to gravity rather than those for two Ising models. To check our observations with a simulation requires the definition of a flip move in the space of quadrangulations, that possesses all the nice ergodicity properties of the standard triangle flip moves. In [11] we baldly presented one candidate move, shown again in Fig.1, without any discussion of its derivation or ergodicity properties. We now remedy this lacuna.

The easiest approach to take is to break our quadrangulation into a triangulation and reconstruct the possible moves from that. We shall consider undecorated (no spin) quadrangulations first. Not every triangulation can be paired off to give a quadrangulation, we need one that admits a perfect matching. A matrix model to do just this (in the dual ϕ^4/ϕ^3 picture) was discussed in [14]

$$Z = \int D^{N^2} \phi \exp - \left(\frac{1}{2} \phi^2 - \frac{1}{4N} e^{\ln 2 - \mu} \phi^4 \right) = \int D^{N^2} \phi D^{N^2} u \exp - \left(\frac{1}{2} \phi^2 + \frac{1}{2} u^2 - \frac{1}{\sqrt{N}} e^{-\mu/2} \phi^2 u \right) \quad (11)$$

where both ϕ and u are $N \times N$ hermitian matrices. Integrating out u on the right hand side gives back the single matrix model on the left hand side. If we go back to the direct lattice picture of triangles and squares the effect of the integration in the above dual lattices is to pair off all triangles into squares. If we look at the dual ϕ^4 diagram to two adjoining squares it can be broken down, or perhaps more correctly exploded, in four possible ways with the insertion of u propagators as shown in Figs.2. The standard ϕ^3 flip moves can be performed subject to the constraint that every vertex must retain one u and two ϕ edges, before collapsing the u propagators to obtain the final ϕ^4 diagram. Performing the allowed flips on Figs.2c,d leave the final ϕ^4 diagram unchanged and the results of the allowed flips on Figs2a,b are shown in Fig.3a and Fig.3b. Just as in the ϕ^3 flip move both labellings of the central segment appear with equal probability in both the diagrams, and just as for the ϕ^3 flip the distinction disappears when one returns to the direct lattice.

When decorating the lattice with spins it is best to think of the spin at the exploded vertices living on the u propagator and getting carried with it in any flip moves. This avoids any potential conflict that might arise when collapsing the diagram after performing the flips if we actually created new spins on the split vertices. The net result of all of this is that the flip moves deduced by the procedure of exploding the ϕ^4 diagram into ϕ^3 diagrams and carrying out ϕ^3 flips before reconstructing the ϕ^4 diagram are precisely those given in Fig.1. Both the moves appear with equal probability. As we can trace the moves back to the ϕ^3 picture (albeit with two sorts of propagators) the ergodicity is assured.

A final subtlety to consider before launching into the simulations proper is the choice of class of quadrangulation. We restrict ourselves for reasons of computational simplicity to non-degenerate quadrangulations in which we do not allow such nasties as squares touching on more than one side. In the dual ϕ^4 picture this corresponds to excluding bubbles on propagators, the “setting-sun” diagram and the one loop contribution to the ϕ^4 vertex. Recent simulations on ϕ^3 graphs have shown, rather counterintuitively, that including the ϕ^3 counterparts of such diagrams actually improves the scaling behaviour and we hope to return to this issue for quadrangulations in further work.

2 Simulations

We simulate graphs of size $N = 100, 225, 400, 900$ and 2500 vertices. In all cases the starting configuration was taken to be a regularly quadrangulated torus for simplicity (e.g. $2500 = 50 \times 50$). The topology of the manifold on which the spin model lives is not expected to change the KPZ/DDK exponents for the spin model transition, although γ_{string} , which we do not measure here, will of course depend on the topology. We conducted 10,000 equilibration sweeps and 50,000 measurement sweeps for most of the lattice sizes at each β value simulated, with more sweeps on the larger graphs and closer to the phase transition. For the ferromagnetic model we updated the spins with the Wolff cluster algorithm, ensuring that on average every spin was updated per sweep. The number of flip updates per sweep was chosen to be equal to N , a rule of thumb that works well for ϕ^3 graphs and triangulations, and seems to do so here too. Varying the number of flip updates by a factor of two in either direction had little effect on the measured quantities. Although it is possible to construct a cluster algorithm for the antiferromagnetic model as well, we contented ourselves with an old-fashioned Metropolis update in this case, again for simplicity as very high accuracy was not a primary requirement.

We measured all the standard thermodynamic quantities for the model: the energy E , specific heat C , magnetization M , susceptibility χ and various cumulants. A short word is in order on the magnetization and energy measurements for the antiferromagnetic model. The normalization of the energy (ie the constant term in the hamiltonian) is chosen so that the energy runs between 2 and 4 for both the ferromagnet and antiferromagnet. In Fig.4 we plot the energy in both models. It is clearly essentially identical, especially when the less efficient algorithm employed for the antiferromagnet is taken into account. This provides the first confirmation of the matrix model result that the antiferromagnetic transition should be identical to the ferromagnetic transition on dynamical quadrangulations. We have to work slightly harder to demonstrate the equality of the magnetizations as the standard magnetization will clearly stay zero in any antiferromagnetic transition. It is, however, still possible to easily define a staggered magnetization on the dynamical quadrangulation because of our choice of starting configuration. We can assign an initial sign or parity to each vertex in a “checkerboard” pattern consistently on the initial regularly quadrangulated torus. The flip move of Fig.1 maintains the parity of flipped links as is clear from looking at the solid and open dots in the diagram, so we can define a staggered magnetization

as

$$M = \frac{1}{N} \sum_{ij} (-1)^{i+j} \sigma_{ij} \quad (12)$$

where i, j labels the original horizontal and vertical coordinates of the spin in the starting torus. Although our choice of a regular torus as starting point makes the definition of the staggered magnetization particularly easy, it should be stressed that *any* loosely packed lattice could be checkerboarded in such a manner and that the corresponding flip moves would not disrupt these assignments or the definition of the staggered magnetization. In Fig.5 we plot the standard magnetization for the ferromagnet and the staggered magnetization for the antiferromagnet, which are again very nearly equal until the inefficiency of the metropolis algorithm begins to bite in the low temperature phase. Note the large error bars in this case; all the other error bars are smaller than the symbols.

Having convinced ourselves of the qualitative similarity of the ferromagnetic and antiferromagnetic transitions from these figures we now proceed to a more quantitative scaling analysis. We commence by looking at the Binder's cumulant for the magnetization

$$U_M = 1 - \frac{\langle M^4 \rangle}{3 \langle M^2 \rangle} \quad (13)$$

whose crossing point for different lattice sizes determines β_c . The data for both the ferromagnet and antiferromagnet give quite clean crossings that are consistent for the various different size pairings, in contrast to our ϕ^3 simulations in [4] where we had to resort to a slightly more devious approach to extract a reliable estimate for β_c . We find $\beta_c = 0.398(2)$ for the ferromagnet and $\beta_c = -0.40(2)$ for the antiferromagnet, where the larger error in the latter is due to the poorer statistics of the metropolis algorithm employed. Note that we have not found $\beta_c = -1/2 \log(3/5) \simeq 0.255 \dots$ as given by the matrix model because the matrix model calculation implicitly assumes the inclusion of the degenerate squares that we have expunged. It would be an interesting exercise to calculate the expected β_c for our variant analytically to compare with the measurements above.

We can extract the combination νD from U_M in various ways. One possibility is to look at the maximum slope of U_M , which is expected to scale as

$$\max \left(\frac{dU_M}{d\beta} \right) \simeq N^{1/\nu D}. \quad (14)$$

For the ferromagnet we find that $1/\nu D = 0.31(5)$ or $\nu D = 3.2(5)$, where the rather large error bar is accounted for by the effect of the smaller lattices. Fitting to only the larger lattice sizes gives both a slightly smaller estimate and a smaller error. If we accept the likelihood of finding KPZ/DDK rather than Onsager exponents the hyperscaling relation $\alpha = 2 - \nu D$ would give us $\nu D = 3$ rather than $\nu D = 2$. The above value is clearly in better agreement with the KPZ/DDK result than the Onsager result. An alternative is to look at the scaling of the slope at the crossover point, which gives slightly a slightly better fit of $1/\nu D = 0.31(3)$ or $\nu D = 3.2(3)$, consistent with the above values. The results for the antiferromagnet are very similar, again with larger errors due to the poorer statistics. Given νD and β_c we can now proceed to a finite size scaling analysis of some of the other exponents. In the discussion which follows, the results are for the ferromagnet unless explicitly indicated otherwise.

Although a fit to the finite size scaling relation for the specific heat is not particularly illuminating because of the extra adjustable constant A that is present

$$C \simeq A + BN^{\alpha/\nu D} \quad (15)$$

it is consistent with the values of νD coming from the cumulant. The specific heat for the ferromagnet plotted in Fig.6 (that for the antiferromagnet is identical) clearly shows the expected cusp, the weak growth of the peak for small lattice sizes dying away as the size is increased. Working in lexicographic order, we now turn our attention to the exponent β

$$M \simeq M_0 N^{-\beta/\nu D} \quad (16)$$

which appears to give rather poor fits on modestly sized ϕ^3 lattices [4], although the use of a triangulation [3] or the inclusion of tadpoles and self-energies greatly improves matters [7]. With quadrangulations we

find that we have maintained our traditionally atrocious fits to β , finding $\beta/\nu D = 0.075(2)$, which translates to $\beta = 0.24(3)$ rather than the KPZ/DDK value of 0.5. The fits to γ from the susceptibility χ

$$\chi \simeq \chi_0 N^{\gamma/\nu D} \quad (17)$$

are much more satisfactory, however. We find $\gamma/\nu D = 0.72(2)$, which using our best fitted value of $\nu D = 3.2(3)$ gives the estimate of $\gamma = 2.3(3)$ in quite good agreement with the KPZ/DDK value of 2. We can see clearly the sharp divergence in χ in Fig.7. A similar story holds for the antiferromagnetic simulations: a good fit to the KPZ/DDK value for $\alpha/\nu D$ is still possible because of the constant term, we find $\beta/\nu D = 0.078(2)$ – again too small, and $\gamma/\nu D = 0.73(7)$.

The lattices we simulate are rather modestly sized, but it is still possible to do a direct fit to the dependence of C, M and χ on the reduced temperature $t = |\beta - \beta_c|/\beta_c$ on the largest lattice ($N = 2500$) as a consistency check. If we fit

$$C \simeq A' + B't^{-\alpha} \quad (18)$$

we again get a good value $\alpha = -1.1(1)$ because of the extra constant A' . The fit to β

$$M \simeq M'_0 t^\beta \quad (19)$$

is even more mediocre than the finite size scaling fit for $\beta/\nu D$, giving a wide range of values with similar goodness of fit depending on the points deleted from the fit. The direct fit to γ

$$\chi \simeq \chi'_0 t^{-\gamma}, \quad (20)$$

on the other hand, is very good: $\gamma = 2.07(2)$.

For completeness we list our fitted exponents and critical temperature for the ferromagnetic simulations below along with the analytical values for the critical exponents

	α	β	γ	νD	$\alpha/\nu d$	$\beta/\nu d$	$\gamma/\nu d$	β_c
<i>measured</i>	-1.1(1)	...	2.07(2)	3.2(3)	-0.35(2)	0.075(2)	0.72(2)	0.398(2)
<i>theory</i>	-1	1 / 2	2	3	-1/3	1 / 6	2 / 3	...

Table 1: Measured and Theoretical values of $\alpha, \beta, \gamma, \nu D$.
(We have not included the very poor direct fit to β .)

We close with a few observations on the efficiency of the Monte-Carlo algorithms. Previous work on triangulations and ϕ^3 graphs has shown that although cluster algorithms greatly reduce critical slowing down for energy observables the magnetization still has quite large values of the dynamical critical exponent z [8], defined through the scaling of the appropriate autocorrelation time τ

$$\tau \simeq N^{z/D}. \quad (21)$$

For the ferromagnetic simulations with the Wolff cluster algorithm we find $z_M/D = 0.39(3)$ for the magnetization, and $z_E/D = 0.23(4)$ for the energy. These values are unlikely to be particularly accurate because of the small lattice sizes, but the value for the energy is unusually large compared with previous ϕ^3 and triangulation simulations. A glance at the metropolis simulations for the antiferromagnet shows that the cluster algorithm autocorrelation times are an order of magnitude better for the magnetization and a factor of two or three better for the energy on the $N = 2500$ graphs, so they still offer an improvement over a local algorithm in spite of the anomalously large z_E .

It was suggested in [8] that the bottlenecks that appear in the baby universe structure of the ϕ^3 graphs and triangulations impeded cluster formation and was responsible for this relatively poor performance. Although we have not investigated the baby-universe distribution of our quadrangulations there is no reason to suppose it is significantly different from triangulations as we are clearly simulating the same continuum theory if the Ising results are to be believed. We would therefore expect the same bottlenecks to be present on our quadrangulations, causing the same obstacles to cluster growth. By the same token, it would be equally easy to perform baby universe surgery [6] on a quadrangulation to help alleviate the problem, the only difference from a triangulation being that the minimum neck is now of length four rather than three.

Other geometrical features such as the flip acceptance as a function of temperature and the cluster distributions look qualitatively similar to earlier ϕ^3 and triangulation simulations. As an additional measure to improve our measurements of the magnetization critical exponent it would be a relatively easy matter to include degenerate quadrangulations in the class of graphs we simulate in order to improve the convergence to the continuum limit.

3 Conclusions

Modulo the usual rather poor fits for the magnetization exponent β the measured critical exponents for “square gravity” are consistent with the KPZ/DDK values, thus providing further explicit numerical support for the notion of universality on dynamical lattices as far as the ferromagnetic transition is concerned. As a by-product of the simulations we have also found the critical temperature for the non-degenerate quadrangulations that we considered here $\beta_c = 0.398(2)$. This translates to the dual value $\beta_c \simeq 0.486$ on non-degenerate ϕ^4 graphs, to be compared with $\beta_c \simeq 0.693$ for ϕ^4 graphs in which the various bubbles etc. are allowed.

It is a relatively simple matter to simulate the dual ϕ^4 model as well, but here of course we would no longer find an antiferromagnetic transition. We need to consider loosely packed lattices on which Neel order is possible to observe the antiferromagnetic transition on fixed lattices, which remains the case for dynamical lattices. On dynamical lattices we are summing over some class of loosely packed lattices, which we implement in the simulations with a compatible flip move. From the matrix model and the simulations it is clear that the antiferromagnetic transition survives its coupling to 2d gravity on dynamical quadrangulations and retains the same exponents as the ferromagnetic transition. The antiferromagnet thus provides an amusing example of Neel order surviving on what is essentially a fluid random lattice.

Extending the approach here to investigate other polygonizations is also not difficult. Exploding higher order vertices into ϕ^3 vertices in such models allows a derivation of the appropriate flip moves and weighting factors.

4 Acknowledgements

CFB and DAJ were supported in part by NATO grant CRG910091. CFB is supported by DOE under contract DE-FG02-91ER40672, by NSF Grand Challenge Applications Group Grant ASC-9217394 and by NASA HPCC Group Grant NAG5-2218. DAJ is also supported in part by EC grant CHRXCT930343.

References

- [1] V. A. Kazakov, Phys. Lett. **A119** (1986) 140.
D.V. Boulatov and V.A. Kazakov, Phys. Lett. **B186** (1987) 379.
Z. Burda and J. Jurkiewicz, Acta Physica Polonica **B20** (1989) 949.
V.A. Kazakov, Nucl. Phys. **B (Proc. Suppl.) 4** (1988) 93.
- [2] V.G. Knizhnik, A.M. Polyakov and A.B. Zamolodchikov, Mod. Phys. Lett. **A3** (1988) 819.
F. David, Mod. Phys. Lett. **A3** (1988) 1651.
J. Distler and H. Kawai, Nucl. Phys. **B321** (1989) 509.
- [3] J. Jurkiewicz, A. Krzywicki, B. Petersson and B. Soderberg, Phys. Lett. **B213** (1988) 511.
R. Ben-Av, J. Kinar and S. Solomon, Nucl. Phys. **B (Proc. Suppl.) 20** (1991) 711.
S.M. Catterall, J.B. Kogut and R.L. Renken, Phys. Rev. **D45** (1992) 2957.
- [4] C. Baillie and D. Johnston, Mod. Phys. Lett. **A7** (1992) 1519.
- [5] J. Ambjørn, B. Durhuus and J. Fröhlich, Nucl Phys. **B257** (1985) 433.
D. Boulatov, V. Kazakov, I Kostov and A. Migdal, Nucl. Phys. **B275** (1986) 241.
- [6] J. Ambjørn, P. Bialas, Z. Burda, J. Jurkiewicz, B. Petersson, Phys. Lett. **B325** (1994) 337.

- [7] C. Baillie and D. Johnston, Phys. Lett. **B286** (1992) 44.
 J. Ambjørn, B. Durhuus, T. Jonsson and G. Thorleifsson, Nucl. Phys. **B398** (1993) 568.
 S. Catterall, J. Kogut and R. Renken, Phys. Lett. **B292** (1992) 277.
 M. Bowick, M. Falcioni, G. Harris and E. Marinari, Nucl. Phys. **B419** (1994) 665.
 J. Ambjørn and G. Thorleifsson, Phys. Lett. **B323** (1994) 7.
 J. Ambjørn, G. Thorleifsson and M. Wexler, Nucl. Phys. **B439** (1995) 187.
 M. Wexler, Nucl. Phys. **410** (1993) 337.
 M. G. Harris and J. F. Wheeler, Nucl. Phys. **B427** (1994) 111.
 J-P. Kownacki and A. Krzywicki, Phys. Rev. **D50** (1994) 5329.
- [8] M. Bowick, M. Falcioni, G. Harris and E. Marinari, Phys. Lett. **B322** (1994) 316.
- [9] C. Holm and W. Janke, “The Ising Transition in 2d Quantum Gravity”, hep-lat/9501004.
- [10] W. Beirl and B. Berg, “Is there Quantum Gravity in Two-Dimensions?”, hep-lat/9505002.
 M. Vekic, S. Liu, H. Hamber, Phys. Rev. **D51** (1994) 4287.
- [11] D. Johnston, Phys. Lett. **B314** (1993) 69.
- [12] B. Eynard and J. Zinn-Justin, Nucl. Phys. **B386** (1992) 558.
- [13] T. Morris, Nucl. Phys. **B356** (1991) 703.
- [14] C. Bachas, “On Triangles and Squares”, CERN-TH.5920/90.

Figure Captions

Fig.1 The two possible flip moves on adjacent squares in DQRS both preserve the “checkerboard” order of the ground state. Up spins are shown as solid dots and down spins as open dots.

Figs.2 The possible ways of “exploding” the ϕ^4 diagram dual to two adjacent squares. The u propagators are represented as dotted lines and the ϕ propagators as solid lines.

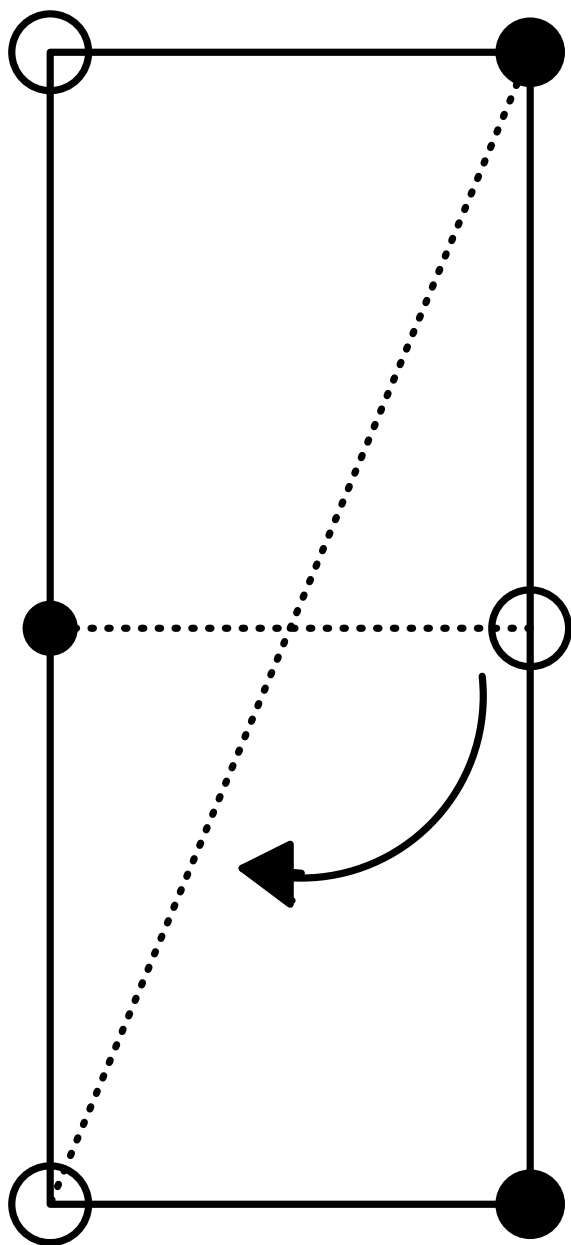
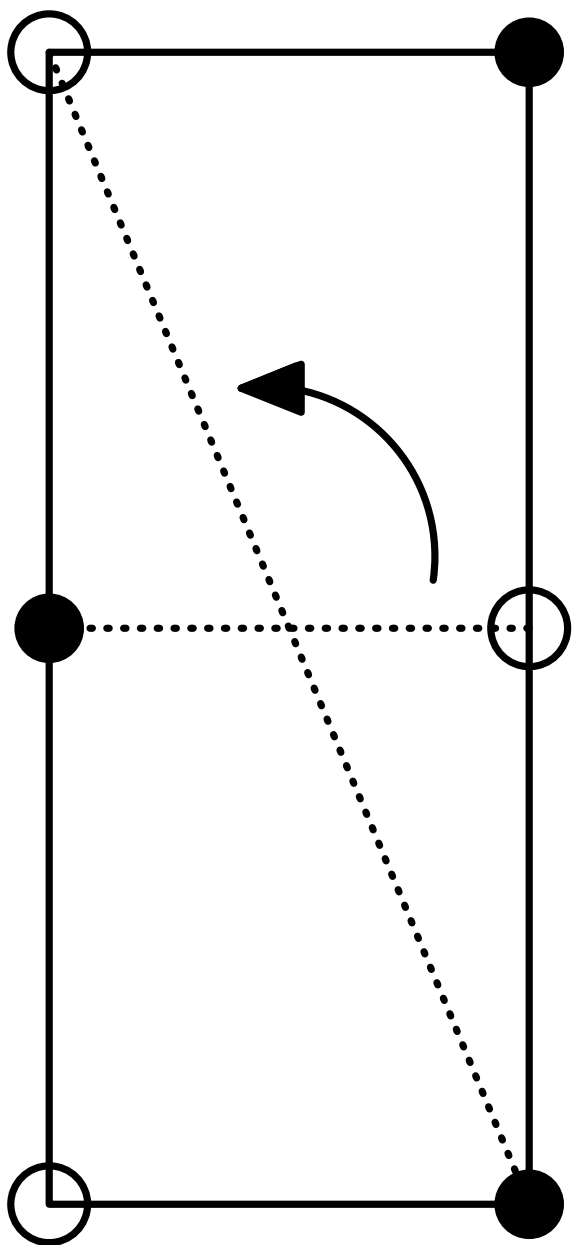
Figs.3 The resulting ϕ^4 flip moves once the diagram has been pieced together again after carrying out all the possible flips in the exploded model. Both orientations of the central link occur with equal probability in both diagrams. Going back to the direct lattice gives the move depicted in Fig.1

Fig.4 The energy for both the ferromagnetic and antiferromagnetic models on the largest lattices simulated ($N = 2500$).

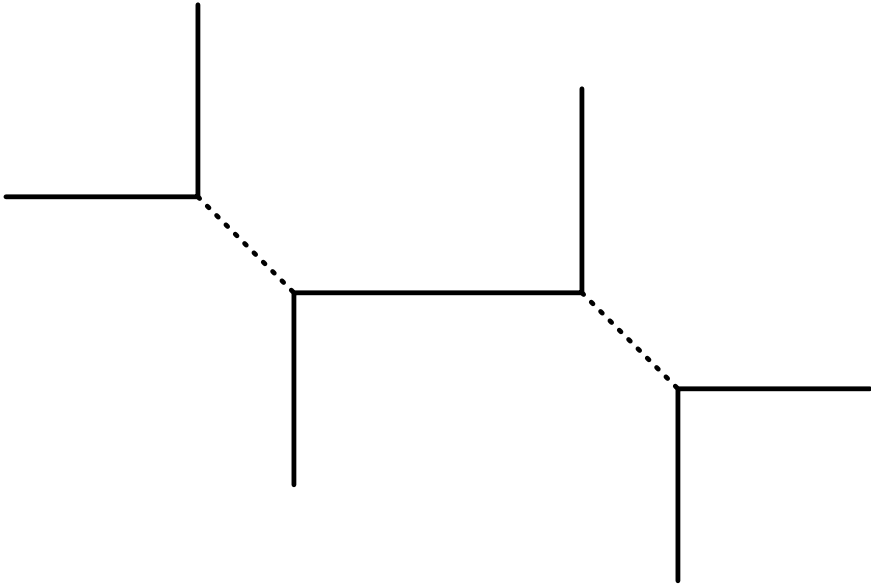
Fig.5 The magnetization for both the ferromagnetic and antiferromagnetic models on the largest lattices.

Fig.6 The specific heat C for the ferromagnet.

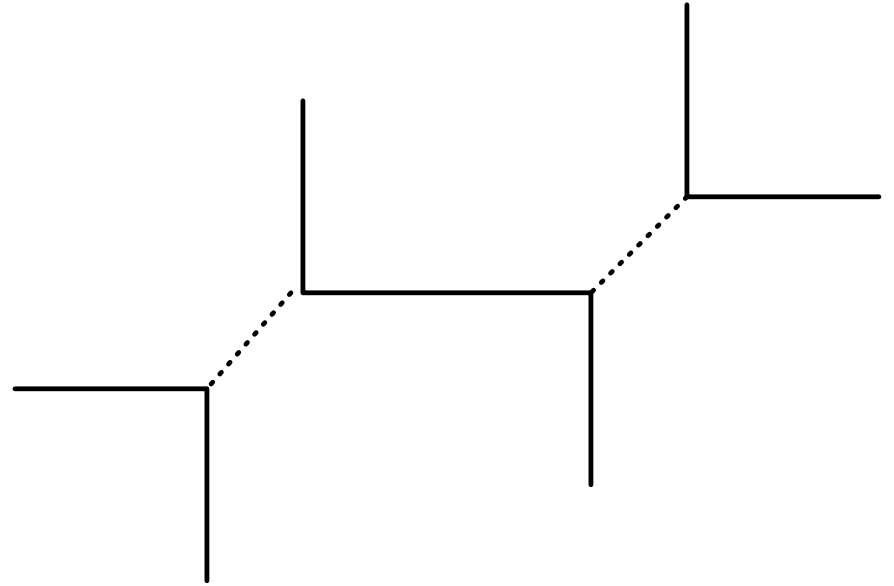
Fig.7 The susceptibility χ for the ferromagnet.



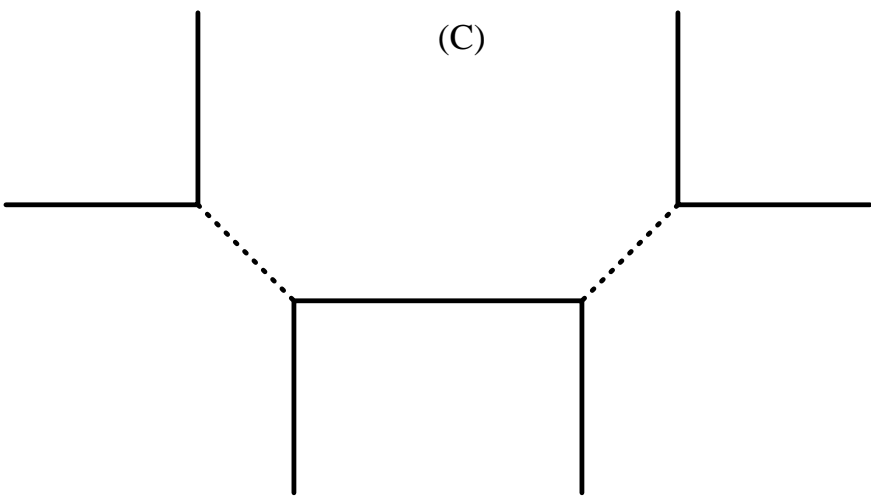
(A)



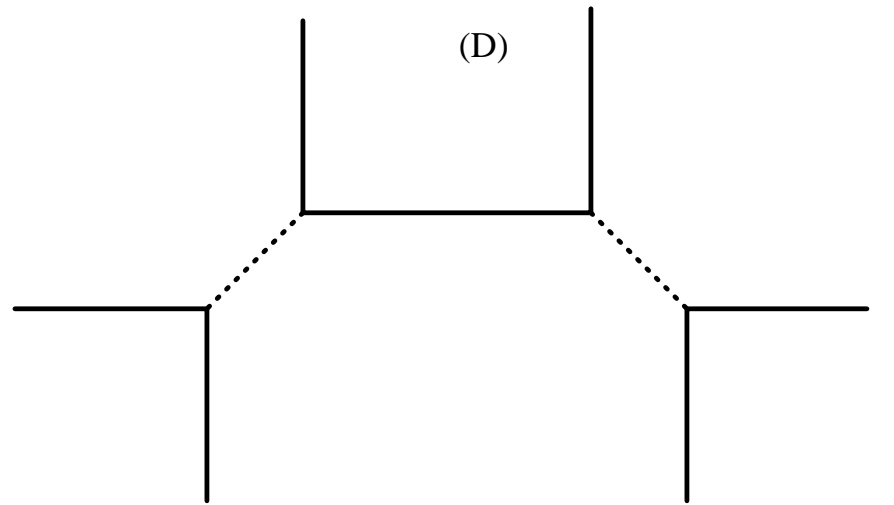
(B)

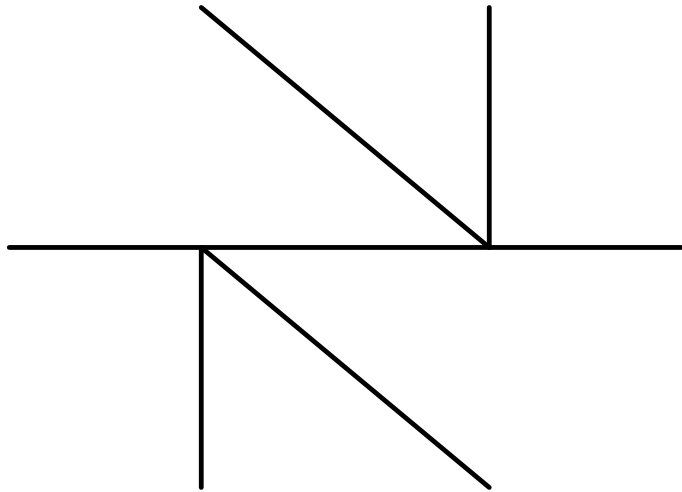


(C)

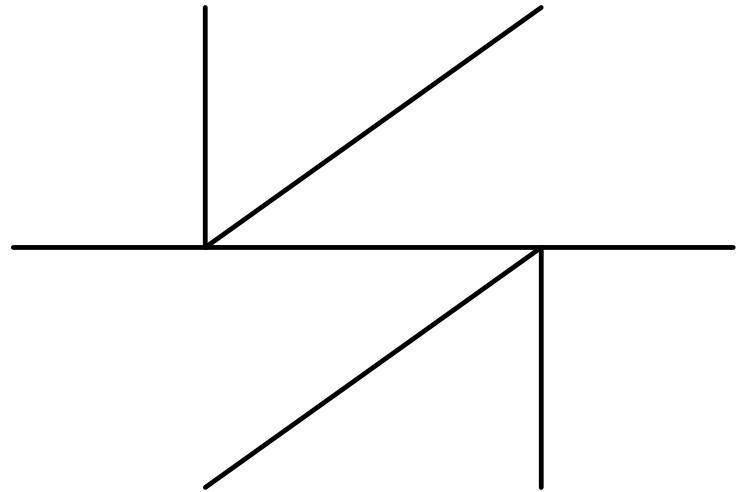


(D)

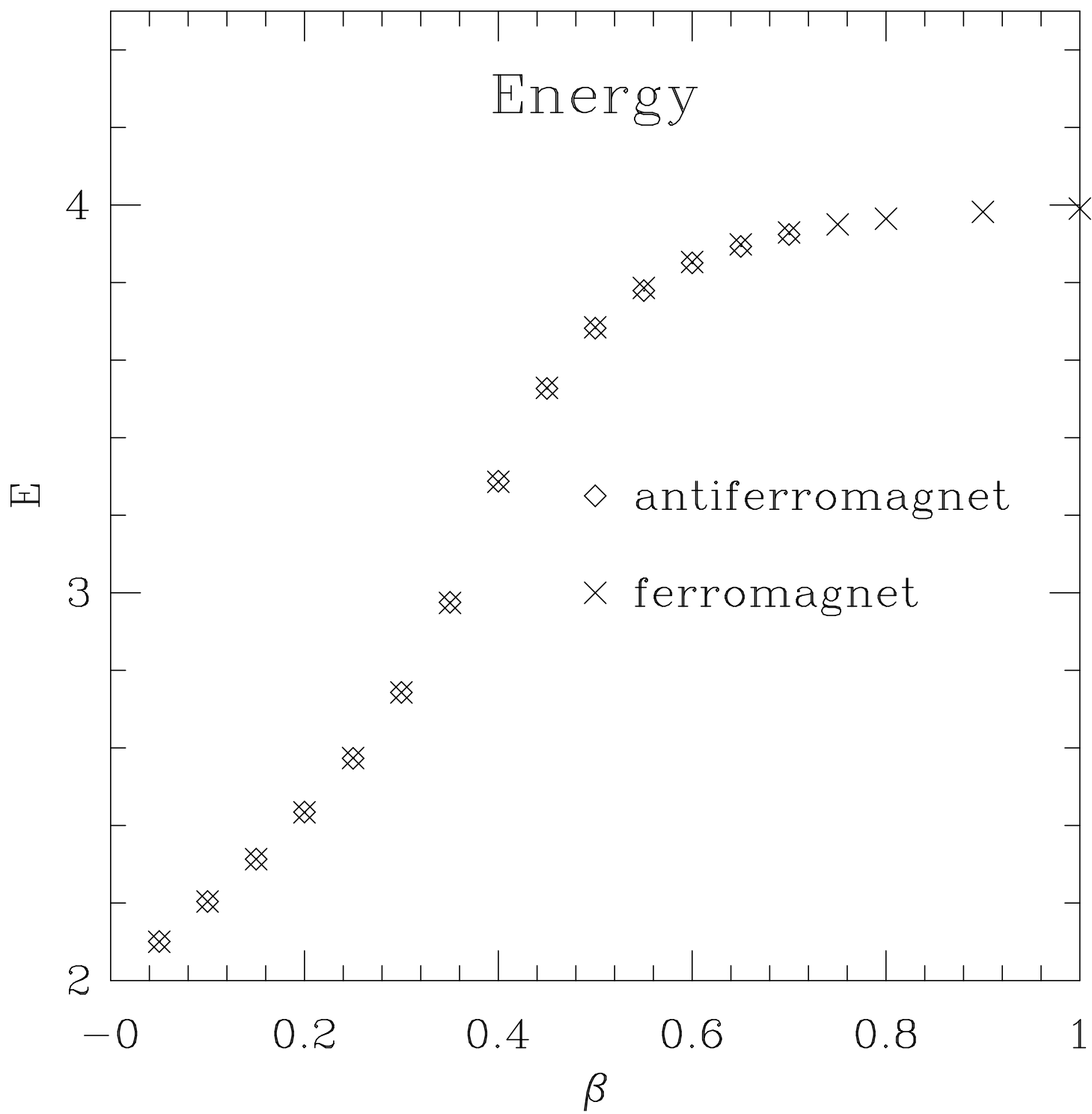




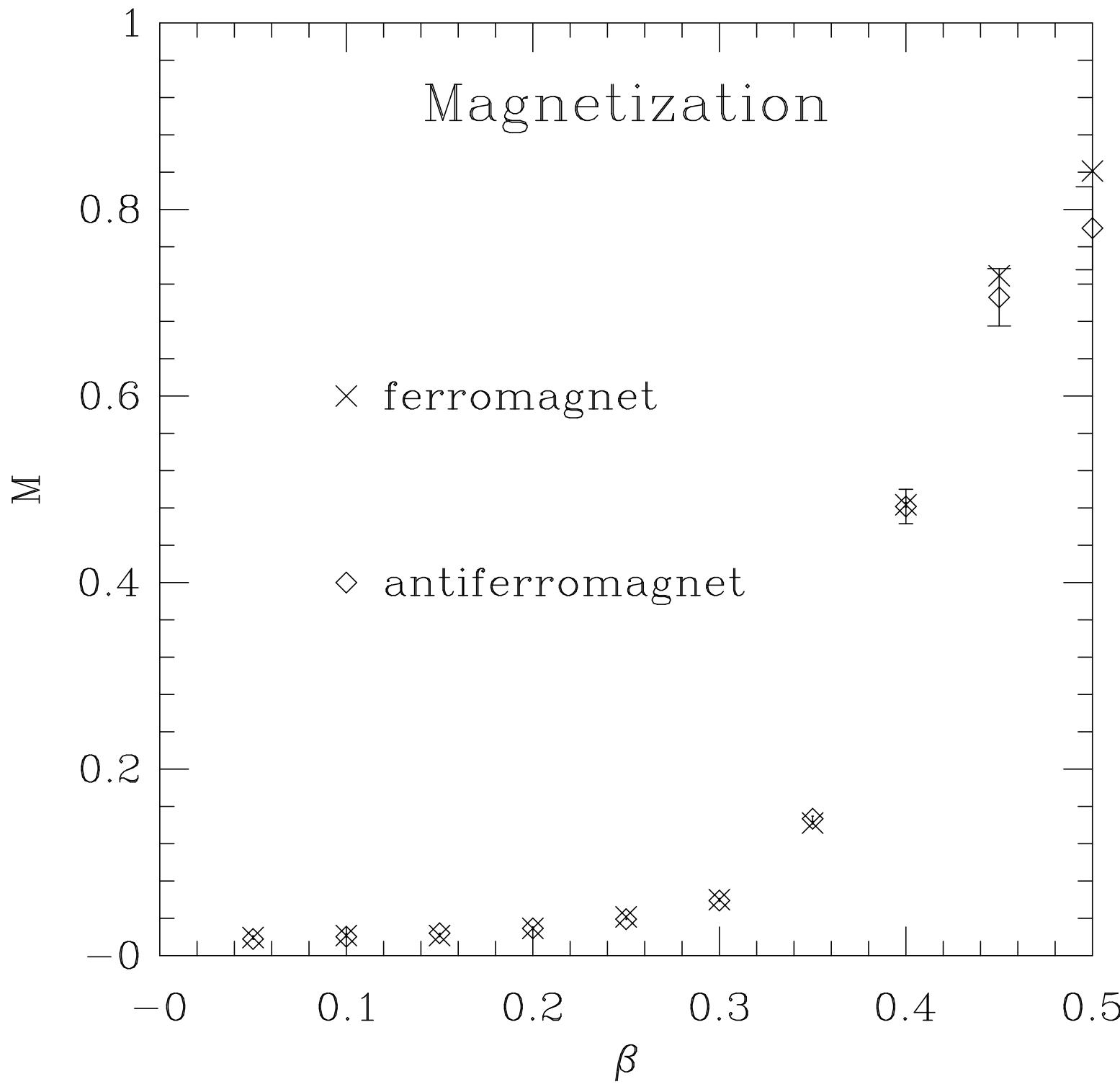
(A)



(B)



Magnetization



Specific Heat

